Remote Sensing of Environment 269 (2022) 112793

Contents lists available at ScienceDirect

Remote Sensing of Environment

journal homepage: www.elsevier.com/locate/rse

Detection of sinkhole activity in West-Central Florida using InSAR time series observations

Oliver-Cabrera Talib [a,*], Wdowinski Shimon [a], Kruse Sarah [b], Robinson Tonian [b]

[a] Institute of Environment, Department of Earth and Environment, Florida International University, Miami, FL, USA
[b] School of Geosciences, University of South Florida, Tampa, FL, USA

ARTICLE INFO

Editor: Dr. Marie Weiss

Keywords:
InSAR
PSI
Sinkhole
GIS
Natural hazards

ABSTRACT

Sinkhole activity in Florida is a major hazard for people and property. Its increasing frequency is often related to an accelerated use of ground-water and land resources in the region. In this work, we use a combined approach of radar interferometry and spatial clustering analysis over three selected sites in West-Central Florida to identify localized deformation that may be caused by sinkhole activity. The region of West-Central Florida is a densely active sinkhole region, where sinkholes tend to be small and land cover is mixed resulting in variable interferometric coherence that complicates Interferometric Synthetic Aperture Radar (InSAR) surveys. In this work, we present a combined methodology implementing InSAR and a Density-Based Spatial Clustering Analysis (DBSCAN) algorithm to detect unknown sinkhole activity and to alert to possible precursors of sinkhole collapse. The data used for the study consist of acquisitions from three TerraSAR-X frames covering time spans of ~1.7 and 2.5 years with spatial resolutions ranging from 25 cm up to 1 m. We applied the Persistent Scatterer Interferometry (PSI) technique using the Stanford Method for Persistent Scatterers (StaMPS) and confirmed the observed deformation signals by also processing the data using the SAR PROcessing tool (SARPROZ). Results show several areas of localized subsidence, from which the cluster with highest rates for each site was selected for detailed inspection. Locations of selected clusters were found in buildings with sizes ranging from 300 m^2 to nearly 2000 m^2, with subsidence trends ranging from −3 to −6 mm/yr. Results were compared with in-situ observations such as ground penetrating radar (GPR), electrical resistivity tomography (ERT) surveys, visual structural inspection and public county archive documents to help as ground truthing; subsiding locations were found to be related to sinkhole presence or development.

1. Introduction

Sinkholes are karstic features formed by movement of rocks or sediments into voids created by dissolution of water-soluble rocks (Dobecki and Upchurch, 2006). Karstic terrain is characterized by evolving rock dissolution and underground drainage (Waltham et al., 2005). Sinkholes can generate holes or collapse when rupture of the rock and soil occurs, and subsidence when a gradual sagging or settling of the surface happens without abrupt rupture (Ford and Williams, 2007). Both cases represent a major hazard to urban and suburban settlements. Development of sinkholes can also drain wetlands or streams and create paths for surface waters to reach aquifers with limited filtering, which can degrade the quality of groundwater resources (Tihansky, 1999). Even though individual sinkholes happen at a local scale (meters to hundreds of meters), they are a hazard with global distribution. Roughly 13% of the Earth's surface its classified as karst terrain (Witze, 2013), and about 25% of the world's population obtains its water from karst aquifers (Youssef et al., 2012). In the United States, damage due to karst subsidence and sinkhole collapse is estimated to be over $304 million per year (Weary and Doctor, 2014; Weary, 2015), highlighting the societal and economic impact of these geological hazards.

Florida is prone to sinkhole activity due to its shallow carbonate deposits, which are susceptible to dissolution by circulating ground water at rates in the range of millimeters per thousand years (Tihansky, 1999). Karst features in much of Florida are covered by a sediment overburden, which collapses or ravels into underlying cavities. Throughout Florida, the overburden layer varies from 0 to 60 m thickness (Fig. 1) (Sinkhole Type, Development and Distribution in Florida, *1985*). While sinkholes form naturally, an increase in occurrence rate is observed in Florida due to accelerated use of ground-water and land

* Corresponding author.
E-mail address: taliboliver88@gmail.com (O.-C. Talib).

https://doi.org/10.1016/j.rse.2021.112793
Received 9 April 2021; Received in revised form 29 September 2021; Accepted 1 November 2021
Available online 18 November 2021

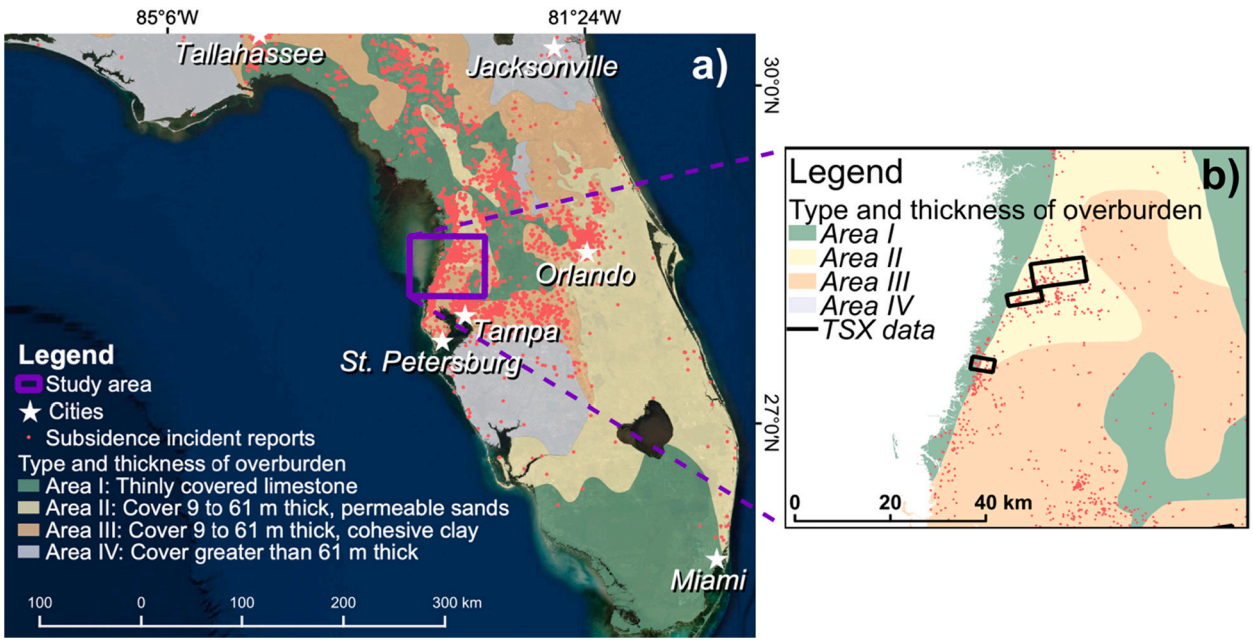

Fig. 1. Sinkhole distribution in Florida. a) Overburden classification map according to type and thickness (Source: Sinkhole Type, Development and Distribution in Florida, 1985) overlaid by subsidence reports in Florida (red dots), collected by the Florida Geological Survey from 1948 to 2017 (Florida Geological Survey, 2015). White stars show the location of the largest cities in the state. Purple frame shows the location of the main study region, presented in (b). b) Enlarged view of the study area in central western Florida showing that the overburden in the three studied sites (black frames) are of type "Area II". Background, ESRI imagery. (For interpretation of the references to colour in this figure legend, the reader is referred to the web version of this article.)

resources together with high precipitation rates. This is a result of anthropogenic structures that promote pond formation and interfere with the normal runoff and drainage dispersion patterns. Likewise, leakage from sewer systems and septic tanks can also impact and promote sinkhole development. (Tihansky, 1999; Veni et al., 2014). The state of Florida alone recorded almost 25,000 sinkhole insurance claims between 2006 and, 2010 (Florida Office of Insurance Regulation, 2010). One of the zones with sinkhole concentration is the west-central region of the state (Fig. 1), the larger sinkhole active zone in central Florida extends over hundreds of square-kilometers and includes three of the most densely populated cities in Florida: Orlando, Tampa and St. Petersburg (Fig. 1).

Detecting sinkhole deformation before a potential collapse is a challenging task, as precursory surface subsidence may be small or unnoticeable. Geophysical methods used to detect sinkholes can provide high-resolution (m to 100 s of m) images of the sediment cover, and in some cases, underlying limestone. Techniques such as ground penetrating radar (GPR), electrical resistivity tomography (ERT), and shallow seismic surveys (refraction tomography, reflection, surface wave inversion) are commonly used to observe and monitor sinkhole activity (Dobecki and Upchurch, 2006; Theron and Engelbrecht, 2018). However, these techniques are limited to relatively small areas (tens to hundreds of m^2), and because of their expense, are typically only used after ground deformation or damage (cracks) to a structure has been observed.

Regional compilations of geological and geophysical information are often used for sinkhole hazard and risk assessments, which are based on modeling and probabilistic approaches (Forth et al., 1999; Galve et al., 2008; Frumkin et al., 2011; Galve et al., 2011; Kim and Nam, 2014; Theron and Engelbrecht, 2018). However, the calculated hazard and risk maps rely on a set of a priori information that for many locations is often incomplete or not available. (15,622 of 24,671 reported insurance claims are clearly associated with sinkhole activity.) In Florida overall, documented sinkhole and subsidence reports have a sparse distribution, covering a wide area (Fig. 1). So, sinkhole detection and monitoring over large regions are impractical using only ground-based methods. Detection and monitoring techniques that allow covering large areas are highly desirable.

Satellite-based Interferometric Synthetic Aperture Radar (InSAR) is a remote sensing technique that has been used successfully to detect sinkhole activity. This method can accurately detect and monitor localized deformation while covering broad areas (Massonnet and Feigl, 1998; Bürgmann et al., 2000; Rosen et al., 2000). InSAR-derived detailed maps of regional and localized deformation can complement the geophysical and geotechnical surveys (e.g., GPR, ERT, borehole data). InSAR observations successfully detected sinkhole-induced deformation in various locations worldwide, including the Ebro Valley, Spain (Gutiérrez et al., 2011), along the Dead Sea shores (Nof et al., 2013, 2019; Atzori et al., 2015; Baer et al., 2018), in Heerlen, Netherlands (Chang and Hanssen, 2014), Gauteng province, South Africa (Theron et al., 2017), in west Texas (Kim and Lu, 2018), Quebec City (Martel et al., 2018) and Prà di Lama, Italy (La Rosa et al., 2018). Sinkhole collapse was also detected by airborne SAR (Uninhabited Aerial Vehicle SAR - UAVSAR) in the Bayou Corne, Louisiana (Jones and Blom, 2013). However, most of these studies were successful in detecting sinkhole-induced deformation because the subsiding and sinkhole related features were previously known or exposed, scattering environments provided a clear view of the features of interest (e.g., Dead Sea shores) and deformation regions are large in size (e.g., West Texas). In contrast, the surface expression of most sinkholes in Florida is small and shallow (meters to tens of meters), making their detection challenging. According to a Florida state subsidence report, the average sinkhole in Florida has a radius of 3.7 m and a depth of 2 m (Florida Geological Survey, 2015). For this reason, in this study we focus on the use of high spatial resolution SAR observations (0.25 to 1.1 m pixel size). The implementation of InSAR alone is not enough to determine the presence of sinkhole-related deformation. Thus, a combined methodology was performed, employing high-resolution radar acquisitions to estimate InSAR time series, together with spatial clustering analysis, to identify sites of potential sinkhole-related subsidence over regions of diverse land cover and rather small sinkhole features. Geophysical surveys and visual observations were then conducted at subsidence clusters

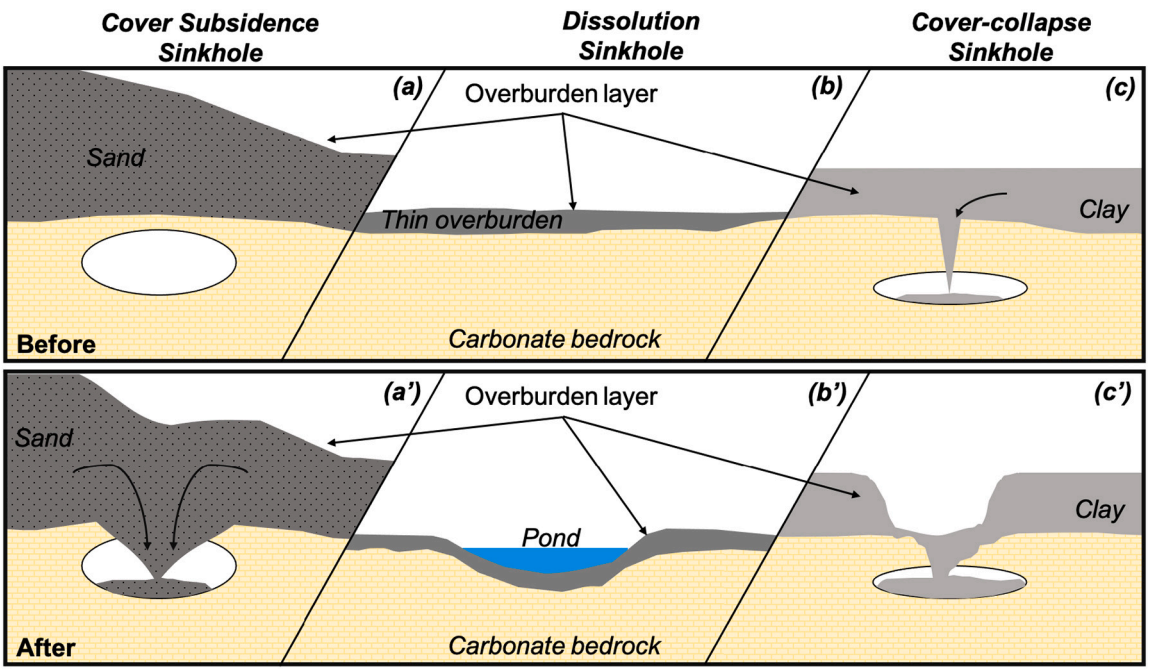

Fig. 2. Schematic stratigraphic cross section showing the relations between overburden layer and sinkhole types. Cover subsidence sinkholes (a and a′) typically develop in sandy overburden layers and dissolution sinkholes develop in thin overburden (b and b′). Cover-collapse sinkhole, less expected within the study area, typically develop in clay overburden shown in (c and c′).

Table 1
Classification of the overburden layer (Sinkhole Type, Development and Distribution in Florida, 1985).

Area Type	Thickness of overburden	Summary
Area I	Bare or thinly covered limestone.	Sinkholes are few, generally shallow, broad and develop gradually. Dissolution sinkholes dominate.
Area II	Cover 9 to 61 m thick; dominant permeable sands.	Consists mainly of incohesive and permeable sand. Sinkholes are few, shallow, of small diameter and develop gradually. Cover-subsidence sinkholes dominate.
Area III	Cover 9 to 61 m thick; cohesive clay.	Consists mainly of cohesive clayey sediments of low permeability. Sinkholes are numerous, of varying size and develop abruptly. Cover-collapse sinkholes dominate.
Area IV	Greater than 61 m.	Consists of cohesive sediments interlayed with discontinuous carbonate beds. Sinkholes are very few, but several large diameter, deep sinkholes occur. Cover-collapse sinkholes are dominant.

for evidence of sinkhole activity. Our cluster analysis on high resolution SAR data proves successful in detecting localized land subsidence above sinkholes, suggesting that the methodology presented here can serve as a useful tool for detecting sinkhole activity, including possible precursors of sinkhole collapse, even in mixed vegetated suburban environments.

2. Study area

Our study area is located in West-Central Florida, where land cover is largely vegetated and suburban. The suburban regions of West-Central Florida are composed of residential homes separated by dense vegetation patches, resulting in a highly heterogeneous scattering environment with variable coherence patterns. Within the study area, we selected three sites based on reported or observed suspicious sinkhole activity (Fig. 1b). Based on the subsidence reports in Florida (Florida Geological Survey, 2015), roughly 17 incidents were reported within a 5 km radius in each study site. The selected sites include open park areas, suburban residential developments, and commercial buildings. The regional geological setting presents conditions for the development of both cover-subsidence and dissolution sinkholes (Figs. 1 and 2) (Full description of the surface stratigraphic units can be found in the supplemental material (S1)). Even though cover-collapse sinkholes are also common in West-Central Florida, based on geological information, they are less expected in the study area (Figs. 1b, 2c and c′). Other important geological information is the type and thickness of the overburden layer. Study sites 1, 2, and the eastern part of site 3 are located on an overburden layer consisting mainly of incohesive and permeable sand with 9 to 61 m thickness (Fig. 1b, Table 1). The western part of site 3 is located on a bare or thinly covered limestone (Area I). Based on the geological setting and the thickness of the overburden layer, it is expected to find in the three sites cover subsidence sinkholes of small diameter, that develop gradually (Table 1). In the western side of site 3, however, the dominant sinkhole type is dissolution sinkholes (Fig. 2b and b′), which are generally shallow, broad and develop gradually.

Our study focuses on the following three sites shown by black frames in Fig. 1:

Site 1: This region is located in Hernando County, centered on the Sand Hill Scout Reservation, and surrounded by suburban developments. The scout reservation is a 1300-acre camp site, mostly undeveloped and used mainly for outdoor activities. The site was selected because ongoing subsidence and structural damage have been observed and clear sinkhole features are present (Robinson et al., 2021). The surface expressions of sinkholes on the Sand Hill Reservation exhibit variable morphologies (Downs, 2017), including steep cover collapse and more gentle cover subsidence sinkholes (Tihansky, 1999). The reservation is mainly covered by grasses and bushes, which result in low interferometric coherence due to the natural rapid changes of the vegetation, such as growth, canopy variations and more (Zebker and Villasenor, 1992). Thus, two Corner Reflector (CR) structures were installed to serve as artificial scatterers in the Scout reservation area to observe surface movement (see Section 4.2).

Site 2: This region is located in Hernando County, south of Site 1,

Table 2
Satellite acquisition information for the three studied sites. HS – High-resolution SpotLight; ST – Staring SpotLight.

Site	Mode	Path	Frame	Time Span (year)	# of images	Rep. Pass (days)	Res. (m x m)
1	HS	29	100	2015.2–2016.9	58	11	1.1 × 0.6
				2017.1–2017.7	11	22	1.1 × 0.6
2	ST	44	15	2015.2–2016.9	45	11	0.25 × 0.6
3	ST	21	38	2015.2–2016.9	54	22	0.25 × 0.6

centered on the Timber Pines development and surrounded by suburban-residential areas. Timber Pines is a private community hosting 3452 homes roughly 60 km north of Tampa. The site was selected because the area has more than 100 subsidence reports and at least 18 confirmed sinkhole-damaged homes have been reported (www.hernandocountygis-fl.us).

Site 3: This region is located in Pasco County centered on the Beacon Woods development ~50 km north-west of Tampa. The frame covers a mix of private developments, small apartment and commercial buildings. This site was selected because more than 30 homes have subsidence reports.

3. Data, processing, post-processing and ground-truthing

3.1. Data

Our data consist of SAR measurements acquired by the TerraSAR-X (TSX) satellite, equipped with an X-band radar sensor (3.1 cm wavelength). Resolutions range between 0.25 and 1.1 m. The SAR images were collected using two different acquisition modes, High Resolution SpotLight (HS) with a resolution of 1.1 m in azimuth and 0.6 m in range and Staring SpotLight (ST) with a 0.25 m resolution in azimuth and 0.60 m range. As shown in Fig. 1b and Table 2, there is a tradeoff between acquisition resolution and coverage area. ST datasets have a smaller coverage area than the one acquired with HS mode (Figs. 1b and 3). We used both acquisition modes in order to evaluate which is more useful for sinkhole detection.

A total of three datasets ranging 45–69 acquisitions were obtained between 2015 and 2018. Each dataset includes 2.5 years for site 1 (ascending), and 1.7 years for sites 2 (ascending) and 3 (descending) with a repeat pass interval of 11 or 22 days (Table 2). During the first acquisition period (2015.2–2016.9), we acquired data over sites 1 and 2 every repeat orbit (11 days) and over site 3 every other repeat orbit (22 days). During the second acquisition period (2017.1–2017.7), we acquired data over site 1 every other repeat orbit (22 days). All the acquisitions for each site were processed to estimate a single InSAR time series per Site. The variation in the repeated pass acquisition frequency is a result of budget constraints, as users of scientific TSX data are

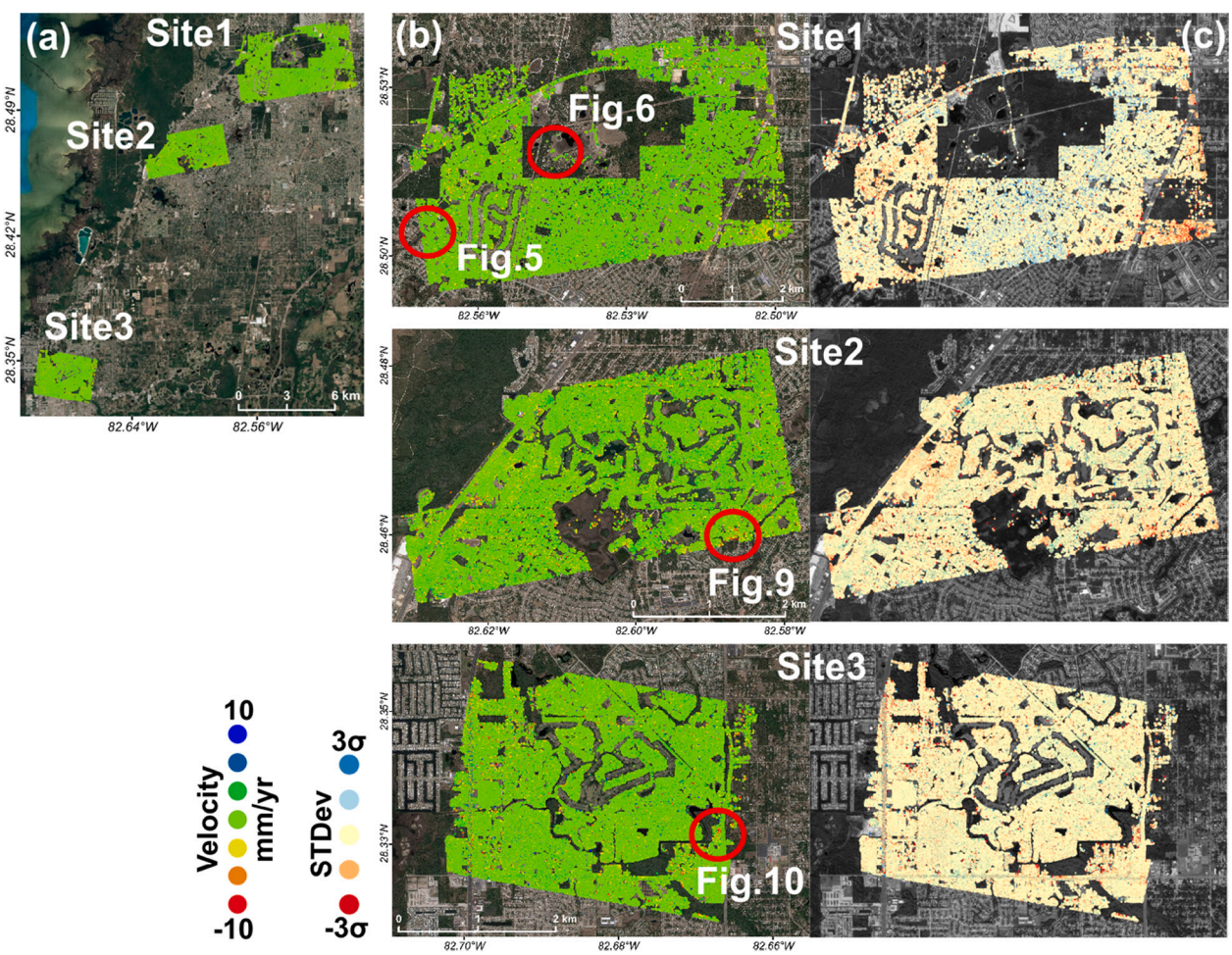

Fig. 3. a) Map of West-Central Florida showing the location of StaMPS PSI results in satellite Line of Sight (LOS). Figures b) and c) to the right show velocity and standard deviation measurements from sites 1, 2 and 3, respectively. The red circles over maps in b) show the locations of subsidence clusters selected for analysis. (For interpretation of the references to colour in this figure legend, the reader is referred to the web version of this article.)

required to pay data production cost.

3.2. Data processing

For each of the three datasets we performed a two-stage analysis. First, we generated a stack of interferograms where all pairs share the same reference image (single reference interferograms). The selected reference was a SAR acquisition with low noise levels and centered, as much as possible, at the middle of the time vector. The SRTM digital elevation model (DEM) was used to remove topography components from the generated interferograms. Since sinkhole size in Florida is typically under 5 m radius, we did not multibook or filter the interferograms to preserve as much detail as possible. After creating a stack of single reference interferograms, they were used as an input for the second stage, time series analysis. We performed the time series analysis through the implementation of the Persistent Scatterer Interferometry method (PSI) (Ferretti et al., 2001). The technique uses scatterers with high backscatter signature (e.g. buildings) and minimizes the use of pixels with backscatter variations, thereby increasing the signal to noise ratio. As a result, displacement time series of individual selected points can be obtained. Constrained by the sensor resolution, sampling acquisition and quality of selected PS points, the accuracy of the PSI technique is usually within sub-centimeter scale and it has been estimated that it can reach precisions of 1.6 to 2.6 mm (Marinkovic et al., 2008). Field observations together with official county ground settlement and reports were used to confirm sinkhole activity in the observed InSAR results.

To generate the interferometric and time series products we used three software packages: Doris (v4.02), developed by the Delft Institute of Earth Observation and Space Systems (DEOS) Delft University of Technology (Kampes et al., 2003), the Stanford Method for PS (StaMPS) (Hooper et al., 2004), and the SAR PROcessing tool (SARPROZ) software package (Perissin et al., 2011). First, we generated a stack of interferograms using Doris (v4.02). Then we use StaMPS to produce a time series of persistent scatterers with stable phase characteristics (Hooper et al., 2004). The use of SARPROZ is simpler, as the software package is a full SAR and InSAR processing tool; it is capable of producing interferograms and PS time series results without the need for extra software. PS selection criteria in this case is based on amplitude dispersion. In both cases the implementation of atmospheric phase screen to reduce atmospheric noise contributions was performed without implementing external models or datasets (more on the software use can be found in supplementary material S5).

Because there are no ground observations to directly validate the InSAR results, we used both StaMPS and SARPROZ software packages to guide data analysis. A similar redundant solution approach has been used for three decades by the precise GPS community for crustal deformation calculations produced by different processing centers and using different processing software packages (e.g., Herring et al., 2016). Each solution will be somewhat different depending on the software algorithms and the user choices of parameter settings for unwrapping, filtering, and accounting for DEM errors. Each solution will have different noise characteristics. The purpose of the solution redundancy is thus not to directly compare the two solutions, but to focus analysis on sites where both solutions detect movements above their respective noise level. These results are more likely to reflect actual crustal movements than movements registered above noise level by only a single solution.

3.3. Data post-processing

The very high-resolution data yielded ~70,000 PS/km^2 for the ST acquisition mode and 7000 PS/km^2 for the HS mode. The vast majority of the calculated PS points indicate relative stability (−1.5 to 1.5 mm/yr) (Fig. 3). Subsiding scatterers are dispersed across the scenes, some reflecting actual subsidence, others reflecting noise, which can be high due to the length of the time series (1.7–2.5 years). We tried various approaches to filter subsiding signal from noise in both temporal and spatial domains. A strictly temporal-based analysis, based on a linear least-square fit of a single or two trend lines at each scatterer, did not yield successful results. A spatial filtering analysis based on a clustering behavior of PS points yielded the best results. The rationale for using a spatial criterion relies on the assumption that sinkhole signals, especially those coming from persistent scatterers on buildings or roads, are expected to be concentrated spatially, when using high spatial-resolution observations. Thus, we conducted a PS distribution analysis to isolate the scatterers that show movement from stable ones. We separate the PS points with negative and positive displacement trends beyond 3 standard deviations (3σ) for the three datasets. Average deformation trends for each site are nearly zero, with standard deviations of 0.6, 0.8 and 0.8 respectively for sites 1, 2 and 3. The applied threshold of 3σ was selected from a range of thresholds between 1 to 3σ and was found most suitable for isolating the PS points that show the largest amount of surface deformation. Those selected points are then used to perform a Density-Based Spatial Clustering Analysis (DBSCAN) algorithm (Ester et al., 1996), to find groups or clusters of moving persistent scatterers based on their spatial distribution. We define a cluster as a group of minimum five PS points that are no more than 6 m apart from each other. The minimum distance criteria of 6 m was chosen because it is double the average sinkhole radius reported in the Florida subsidence reports (Florida Geological Survey, 2015), but closer to the dimension of a residential roof or road.

3.4. Ground-truthing

Ground-based surveys were performed at selected sites, based on the InSAR analysis results, in order to verify that the InSAR-detected deformation was related to sinkhole activity. In one case, however, we conducted the ground-based surveys before acquiring the InSAR data, in order to verify that the corner reflectors were constructed on a subsiding sinkhole in site 1 (Section 4.1). Our ground-based verification was based on the following methods (Robinson et al., 2021):

1) Ground penetrating radar (GPR). GPR is a geophysical technique that uses the reflections of radar waves to image the geometry and internal layering of sediments covering the limestone. Characteristic features in particular indicate the raveling of sand into underlying voids, as in Fig. 2 bottom.
2) Electrical resistivity tomography (ERT). ERT is a geophysical technique that images the subsurface by measuring electric potential differences from currents driven with an array of electrodes. ERT profiles can illuminate heterogeneities and voids in limestone as well as the sediment cover.
3) Visual inspection of structural damage to buildings, mainly inspection of cracks.
4) Inspection of the public county archive for documents containing official sinkhole reports.

Common-offset GPR data was acquired with a Mala ProEx system with shielded 250 MHz antennas mounted on a cart. Trace acquisition was odometer-triggered at 2.3 cm intervals, with a 4-fold stack. Data was processed using Reflexw (Sandmeier Software) with a 4 ns dewow filter, a time-zero correction, a linear gain, and removal of the average trace to reduce system noise. A best-fitting average velocity to ~2.5 m depth was determined from diffraction hyperbola fitting to be 0.085 m/ns for data from Site 2. The velocity was used to perform a Kirchoff migration and time-to-depth conversion. The GPR surveys were conducted on 9/19/2015 for the corner reflector area and on 5/9/2018 for the rest of the study sites.

An ERT line of approximately 140 m in length with 2-m electrode spacing (dipole-dipole Reverse Schlumberger geometry) was completed on 9/18/2015 at the Sandhill Reservation (Site 1) using the Advanced

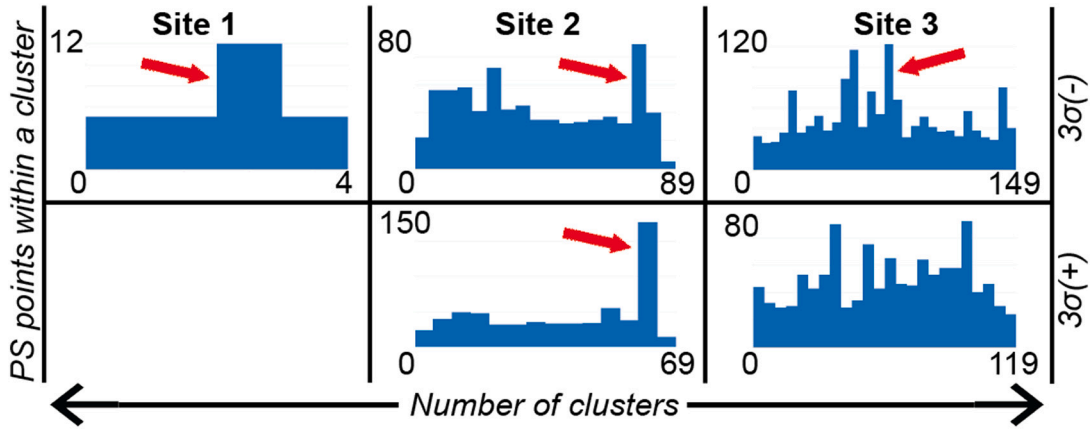

Fig. 4. Results of clustering analysis for the three sites. 3σ negative (up) and positive (down) histograms showing number of PS per calculated cluster in each study site. Red arrows show the cluster with the highest number of PS points in each histogram, shown in detail in Figs. 5, 9 and 10 for subsiding points, and in Fig. S4 in supplemental material for the positive (uplifting) cluster at Site 2. No positive clusters were found in Site 1. (For interpretation of the references to colour in this figure legend, the reader is referred to the web version of this article.)

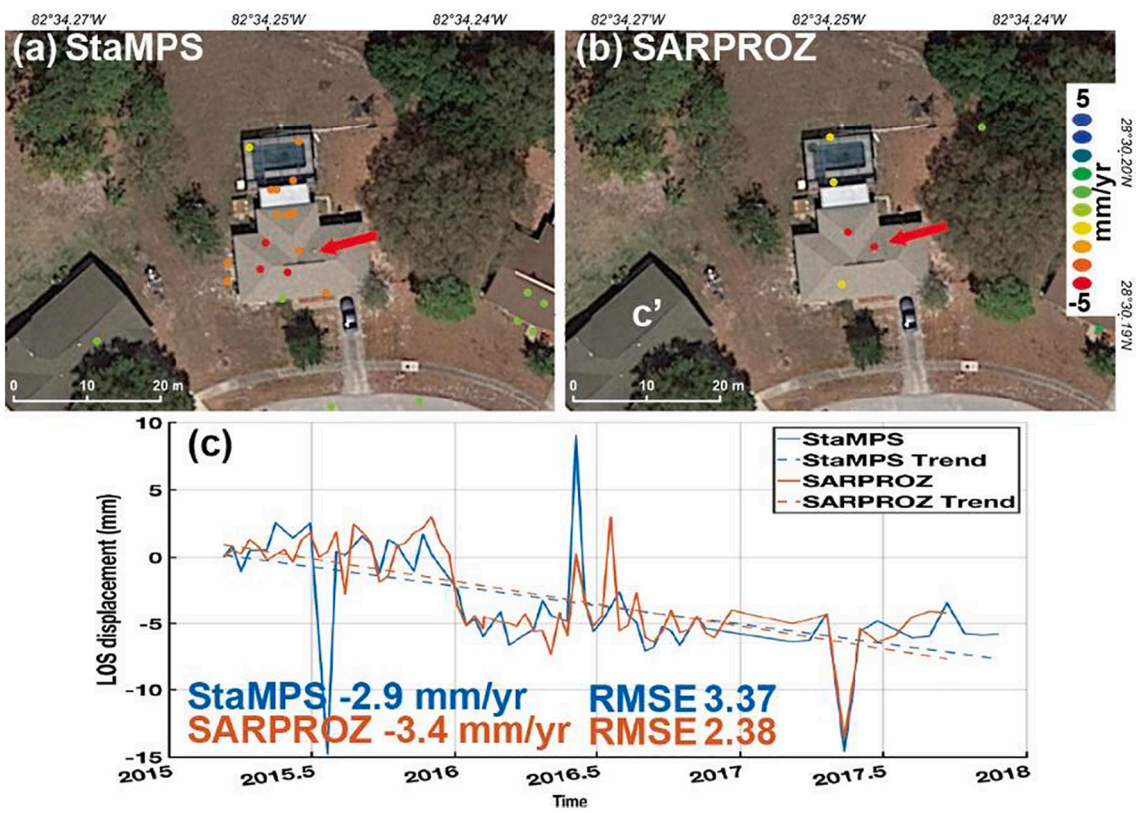

Fig. 5. Velocity map of Site 1 densest negative cluster, determined from TSX HS data covering a time span of 2.5 years and processed by StaMPS and SARPROZ software packages. See Fig. 3 for location. StaMPS results were generated from 44 interferograms; SARPROZ velocity field from 69. a) StaMPS velocity field zoom-in of a subsiding house in Site 1. b) SARPROZ velocity field zoom-in of the same house. c) SARPROZ and StaMPS detected pixel movement time series showing displacement velocity of −3.4 and − 2.9 mm/yr, in Line of Sight (LOS) respectively. The red arrows show the scatterers plotted in c). (For interpretation of the references to colour in this figure legend, the reader is referred to the web version of this article.)

Geosciences, Inc. SuperSting R8-IP Resistivity meter. Simple processing steps were applied to (1) delete outlier points, and (2) invert the data for the earth resistivity structure that produced the lowest misfit between data and model in a least squares sense, using the Res2DinVx32 software (Geotomo Software).

4. Results

Results of StaMPS PSI processing from the three sites are shown as maps of surface velocities and displacement time series of selected points of interest. Velocity maps of all sites indicate stability in most of the region (green colour in Figs. 3, 5, 9 and 10). However, the results also contain many points with high positive and negative velocities (> ±5 mm/yr), which include deformation signals together with the noise

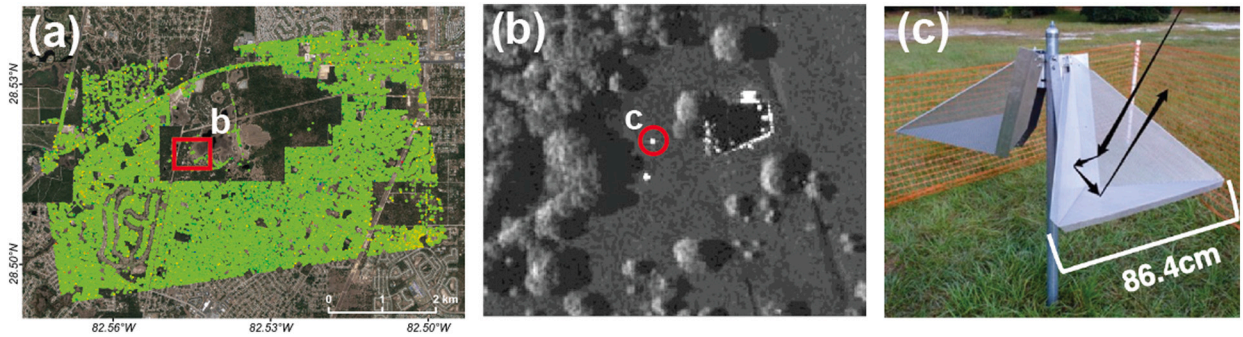

Fig. 6. CR example, location inside the Sand Hill Scout Reservation study area. a) Velocity map of Site 1 showing extremely limited PS coverage over the reservation. b) High resolution Spotlight TSX backscatter zoom-in image of the CR location. The red circle in (b) shows the bright pixel result of the enhanced backscatter from the CR. c) Photo of one of the CRs after installation. The black arrows exemplify the interaction of the radar beam with the CR. (For interpretation of the references to colour in this figure legend, the reader is referred to the web version of this article.)

possibly related to the dataset time span (1.7–2.5 years).

Localized subsidence can be observed by zooming into selected sites (Figs. 5, 9 and 10). These subsiding areas vary in size from approximately 10 m × 20 m, of a single-family house, to 50 m × 60 m, of a small apartment building. Here we present detailed time series observations for a StaMPS and SARPROZ location-matched PS point within each cluster that showed the highest number of subsiding PS points through the application of DBSCAN (Figs. 4, 5, 9 and 10).

The spatial resolution of the PS results depends on both the resolution of the acquired data (HS versus ST acquisition modes – Table 2) and surface scattering characteristics. The PS selection is highly correlated to the amplitude dispersion (Eq. (S3)). Thus, strong variations in backscatter will result in a decrease of PS density. The highly heterogeneous land cover of suburban western central Florida results in variable backscattered intensity. Consequently, the spatial resolution of the PS is much lower than the pixel resolution and is in the range of 5–10 m.

Persistent scatterers with Line of Sight (LOS) movement rates beyond 3σ, both negative (subsiding) and positive (uplifting), were input to the density-based spatial clustering analysis (Fig. 4). Histograms showing the number of PS points per cluster were generated. We selected the clusters with higher PS number in each case to perform detailed observations.

Results from the clustering analysis show that Site 1 has the least amount of localized deformation clusters of all the sites. The 3σ histogram of PS points showing upward movement for Site1 was not generated because no cluster with 5 or more points in a 6 m vicinity was found for that region. Site 2 has 89 subsiding clusters with high PS density, and 69 showing upwards movement with a general lower PS density except for one cluster. A plot of the positive cluster with the largest number of scatterers in Site 2 was generated (Fig. S4 in supplemental material). Results show that the positive clusters present a mix of upward and downward scatterers, providing no reliable information of localized deformation (Fig. S4b). Site 3 shows high density results for both subsiding and uplifting clusters, with 30% more subsiding clusters. As for Site 2, the positive clusters on Site 3 show noisy responses and thus do not provide clear or reliable surface movement information. The selected subsiding clusters are shown in detail in Figs. 5, 9 and 10 with GPR surveys performed at the selected clusters in Sites 2 and 3.

4.1. Site 1

Vicinity of Sand Hill Scout Reservation. Low average deformation rates were obtained on site 1. The four clusters of subsidence identified through the DBSCAN algorithm each cover the extent of an individual house. The central region of the scene shows almost empty PS coverage (Fig. 3 top right) that follows the limits of the Sandhill Scout reservation. The lack of persistent scatterers within the reservation occurs because of the dominant vegetation coverage in the area, which does not provide a stable scattering environment over periods longer than few weeks, and thus low coherence (Zebker and Villasenor, 1992).

Fig. 5 shows the InSAR results at the densest negative cluster at Site 1, showing downwards deformation of approximately 3 mm/yr on the rooftop of a house. The time series of the scatterers plotted display a step-like downward movement toward the end of 2015 and abrupt phase jumps in the middle of 2016 and 2017 (Fig. 5c). Detected velocities from neighboring houses are mostly stable, in the order of +/- 1 mm/yr for both SARPROZ and StaMPS. Both velocity maps in Fig. 5 cover the same time span of observed deformation; however, StaMPS results were generated from 44 interferograms, 25 less than the used in SARPROZ. This difference is due to pulse repetition frequency (PRF) variations in the SAR acquisitions, introducing noise to some of the interferograms and unable to be corrected within StaMPS forcing the exclusion of those InSAR products, whereas SARPROZ was able to process all acquisitions and correct for the (PRF variations).

Inspection of the public Hernando County archive records show that this property has undergone stabilization, an engineering process typically initiated in response to structure subsidence. Repair works occurred toward the end of 2015, which also matched the abrupt movement observed on the InSAR results.

4.1.1. Corner reflectors installed at Site 1

Two corner reflector (CR) structures were constructed on a topographic low in an open vegetated area in Site 1 in October 2015, in order to serve as artificial scatterers (Fig. 6). The area has documented sinkhole activity, as described below. The CR design criteria were set to meet the characteristics of the X-band signal. Theoretical considerations suggest that the CR effectiveness increases with its dimension and, hence, promote the use of large CRs (Garthwaite et al., 2015). However, in order to minimize the CRs' weight on the supporting pole and reduce the effect of strong winds on movement, a smaller size is desired. Based on the above considerations, 86.4 cm CRs were chosen for the project (Fig. 6). The CR's main body is made from 0.063 × 1/8 perforated aluminum sheet (36″ x 36″). Four corner reflectors were installed on two poles, two directed toward signal transmission in ascending and the other two toward transmission in descending orbits of the X-band satellites.

One set of reflectors was constructed near the center of the ~60 m-diameter, 1.6 m-deep topographic low, and the other 20 m to the northeast, within but on the flank of the depression (Fig. 8b). Time series results were obtained using SARPROZ because it was possible to use the whole available interferograms due to the PRF variations. The software provides a small area processing module that allows quick analysis of small portions of the SAR acquisitions, which was very convenient for analyzing CR behavior.

The reflectors improved echo returns from the grassy field; this is observed in noise reduction in the displacement estimates after they

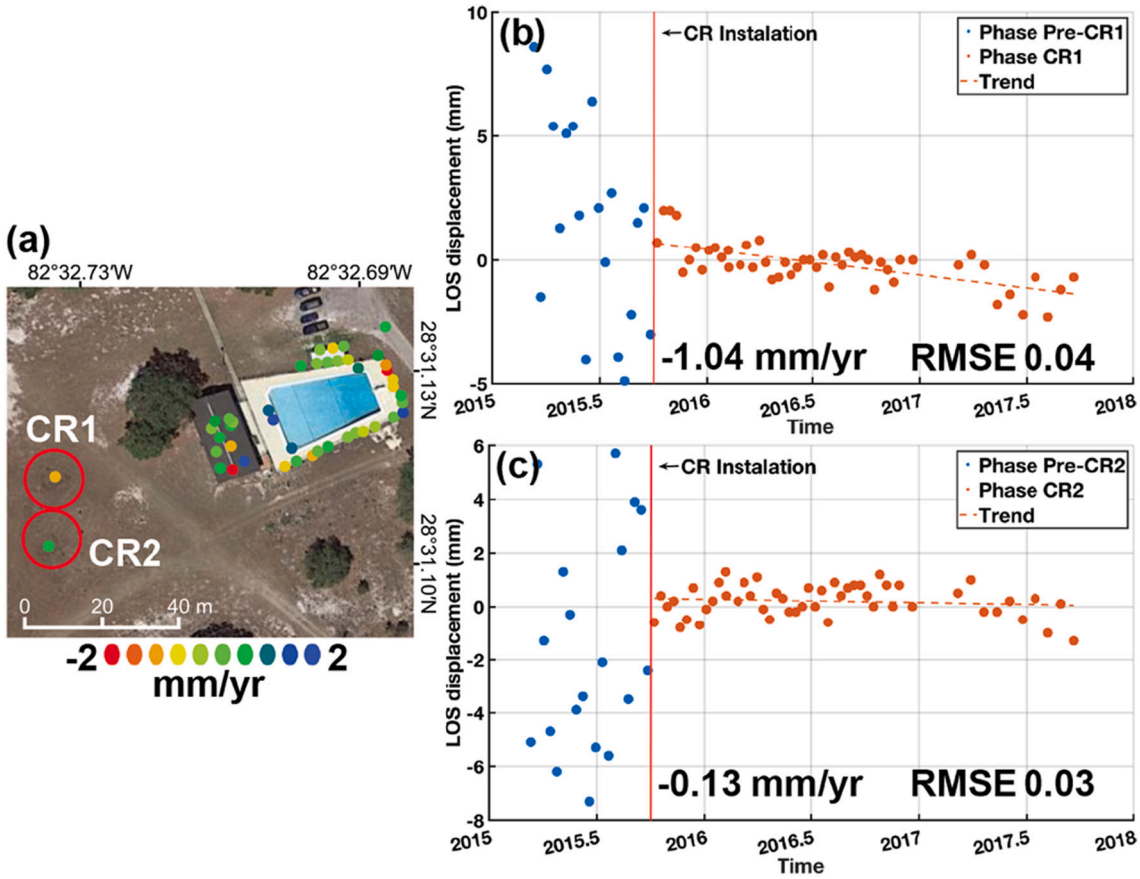

Fig. 7. SARPROZ analysis of corner reflectors installed in the Sandhill Scout Reservation (location shown in Fig. 6). a) Zoom-in of satellite image showing PS in the CR study area located near the swimming pool. b) Time series detected from corner reflector 1 in Site 1 with root mean square error (RMSE) of 0.04. c) Time series detected from corner reflector 2 in Site 1 with RMSE of 0.03. Vertical red line in both b) and c) indicate the CR installation date. (For interpretation of the references to colour in this figure legend, the reader is referred to the web version of this article.)

were installed (Fig. 7b and c). The effectiveness is evaluated by computing the Signal to Cluster Ratio (SCR) in the supplemental material (Eq. (S2)) (Freeman, 1992). The northeastern CR, on the flank of the topographic low, has an average velocity of −1.04 mm/yr over the ~2-year measurement span, while the apparent motion of the CR in the topographic low averages only −0.13 mm/yr, a rate below the RMS uncertainty. We note both rates are significantly lower than the rates of the 'cluster' sites described above.

Sinkhole-related subsidence at the Sandhill Scout Reservation has been documented by visual observations over the last two decades (B. Rodgers, P.G. pers. Communication). In 2014 cracks formed in the building and the swimming pool adjacent to the topographic low (Fig. 9). Boreholes drilled on the eastern edge of the swimming pool just 10 m apart showed in one case ~10 m of sand over limestone, and in the other ~20 m of sand over limestone (Fig. 10 B1 and B2) (Robinson et al., 2021). These dramatic differences in depth to limestone are characteristic of cover-subsidence sinkhole environments and are likely associated with the observed swimming pool cracks. A resistivity transect conducted near the pool in September of 2015 (Fig. 10) shows a low-resistivity zone potentially indicative of a saturated sand-filled void. Ground penetrating radar surveys show a highly irregular surface at 4–6 m depth (Fig. 10, red arrows) also suggestive of sinkhole activity. Combined the data suggest that sinkhole activity is complex in time and space, particularly as the CR in the topographic low was stable during the two years of InSAR monitoring, while the flank subsided at ~1 mm/yr.

4.2. Site 2

Vicinity of Timber Pines development. Results obtained by both processing algorithms indicate an overall stability, with some small scattered areas of localized deformation (Fig. 3). Most of the subsiding structures in this area are houses with few larger commercial buildings in the western part of the site. Three subsidence clusters, separated by ~50 m from each other, are located within the red circle shown in Fig. 3 right, middle, and on Fig. 6. Two clusters are in houses and one located in the middle of a paved road approximately 20 m long (Fig. 9). Detailed observations of the deforming pixels along the road show a clear downwards trend reaching -6 mm/yr for SARPROZ and -5 mm/yr on StaMPS. Neighboring scatterers outside the clusters generally show deformation rates less than 1 mm/yr from both processors. Surface observations of sinkhole activity include a semicircular depression ~10 m north of the subsiding section of road (near tip of red arrow on Fig. 9a and b). Similarly, a circular depression several meters in diameter and a half meter in depth is observed southeast of the subsiding road section, adjacent to a home where subsidence is also indicated (Fig. 9e). GPR transects were performed along the road (Transect A, Fig. 9d) and adjacent to one of the houses (Transect B, Fig. 9e). Both profiles show characteristic sinkhole features. These features include 2-3 m deep, infilled depressions up to 20 m in diameter in the karst-mantling sediments (Transect B in Fig. 9; pink and green arrows). Adjacent to this Transect B GPR profile over infilled depressions, three surface depressions of 2–3 m in diameter and tens of cm depth are visible on the site. The combined observations suggest both past subsidence (now infilled) and current active subsidence in these grassy lawn areas.

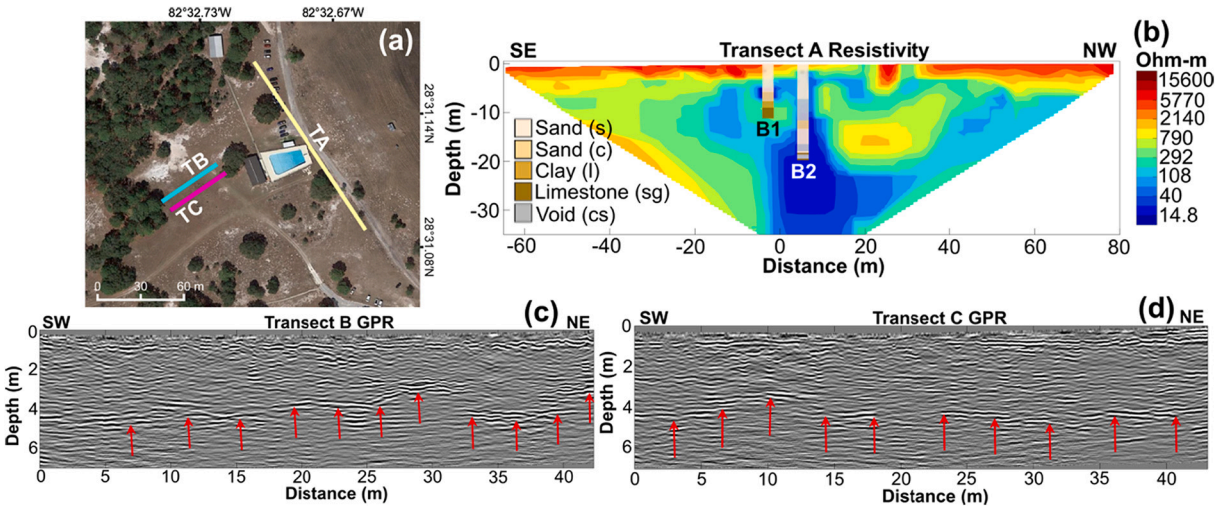

Fig. 8. Ground penetrating radar, resistivity surveys and borehole samples near the site of the CR installations. (b) The transect A resistivity profile located east of the cracking swimming pool shows low resistivity values at the center of the line interpreted as a saturated sand-filled void. Borehole data B1 and B2 is shown overlayed on the resistivity transect. Samples are located roughly 10 m apart showing different limestone depths ~10 m for B1 and ~ 20 m for B2. Corresponding legend is shown to the bottom left corner where abbreviations shown in parenthesis are the following: (s) silty, (c) clayey, (l) limey, (sg) soft-granular and (cs) compressionable sand. Arrows in GPR profiles of transects (b) and (c) show both continuous and discontinuous subsurface reflectors believed to drape the underlying limestone surface.

Beneath the subsiding of road shown in Fig. 9(d), GPR Transect A shows a deeper and broader infilled depression (4 m deep, > 35 m wide) that terminates at the eastern terminus of the subsiding zone (blue arrows in transect A Fig. 9). The GPR-imaged sediment infill of this deeper depression shows a shallow trough indicating more recent subsidence and infill over the central zone (yellow arrows in transect A Fig. 9).

The combined observations suggest irregular and intermittent subsidence of the type associated with sinkhole activity, which has been pervasive in this region. Official county documents (pascocountyfl.net) confirm sinkhole activity in several homes in the surrounding areas, including the ones showing signal in Fig. 9. However, no information regarding dates of subsidence events was found.

4.3. Site 3

Vicinity of Beacon Woods development. Similarly to Site 2, the area is mainly covered by small size houses and a few larger commercial buildings in the southern and western portions. Results from both processing methods show generally stable scatterers. InSAR observations show dense subsidence clusters occur at the Ridgestone Apartments (Fig. 10). Deformation observed from a sample PS point in the building shows subsidence with an overall average velocity of −5 mm/yr in SARPROZ and − 4.6 mm/yr in StaMPS (Fig. 10c) over the 1.7 year period. Both processing software's time series show that the overall average subsidence is dominated by an abrupt drop (~ 4 mm) over the time interval between satellite passes on October 19th (2015.8) and November 6 (2015.85), 2015, followed by a year of relative stability.

The GPR measurements show a 150 m wide and 1.8 m deep depression, indicative of repairs done due to sinkhole presence. The location of peak subsidence rates indicated by the arrow (Fig. 10 a and b) corresponds to a portion of the apartment complex fronted by a tilted sidewalk slab dipping westward toward the apartment. The apartments at the far north-east corner of the apartment complex (Fig. 10a and b) are closed and not used, presumably due to subsidence, while the rest of the complex is inhabited. Official reports from the county (pascocountyfl.net) and the work by Veni et al., 2014, also report the building has or had sinkhole activity; however, no date of report or event was available. The vegetated area directly west of the apartment complex is the site of a local drainage system, suggesting a possible relationship between subsidence and the presence of the drainage.

A 270 m-long N-S GPR survey was run parallel to the apartment complex, 25 m east along the N-S road, to look for indications of sinkhole activity (Fig. 10d). The GPR profile shows a large infilled depression in the surface sediments, almost 2 m deep and approximately 150 m meters long. If this depression has the quasi-circular shape commonly observed at sinkholes, it would be expected to extend beneath the apartment buildings to the west. Together the data suggest that current subsidence may represent a re-activation of earlier subsidence indicated in the GPR profile.

5. Discussion

Results from both processing algorithms used in this study show that the PSI technique effectively detects localized deformation in suburban areas of central Florida. Further discussion on software can be found in the supplemental material S5. Results from the cluster analysis successfully showed regions of sinkhole activity regardless of the noise product of the short observation timespan. Observed cluster deformation represents, in most cases movement of buildings and constructed areas, which can occur due to sinkhole activity, but also by other processes such as shrink-swell soils. Detected InSAR-derived deformation trends from Sites 1 and 3 show step-like downward patterns. For the case of Site 1, this behavior is observed toward the end of 2015 and it was found from property records that the building underwent stabilization works due to sinkhole activity around that time. Similar behavior was observed in Site 3 also toward the end of 2015 (~October–November). Although no official documents or reports were found for Site 3, GPR measurements reveal the observed depression is indicative of repairs done due to sinkhole presence, showing a possible relationship between the observed step-like movement and buildings that have undergone sinkhole repairs. Together the GPR measurements show depressions that range between 2 and 4 m deep and with variable lengths, from a couple of ~5 m features on Site 2 up to 150 m wide on Site 3, exemplifying the variability of sinkholes in West-Central Florida. Field verification is thus needed to determine the cause of InSAR-detected deformation. However, InSAR can be used to monitor large areas for localized subsidence and provide highly valuable warning information and guidance for ground-truthing studies. A combined approach of InSAR and multi-temporal field verification surveys would yield detailed measurements of deformation and sinkhole development.

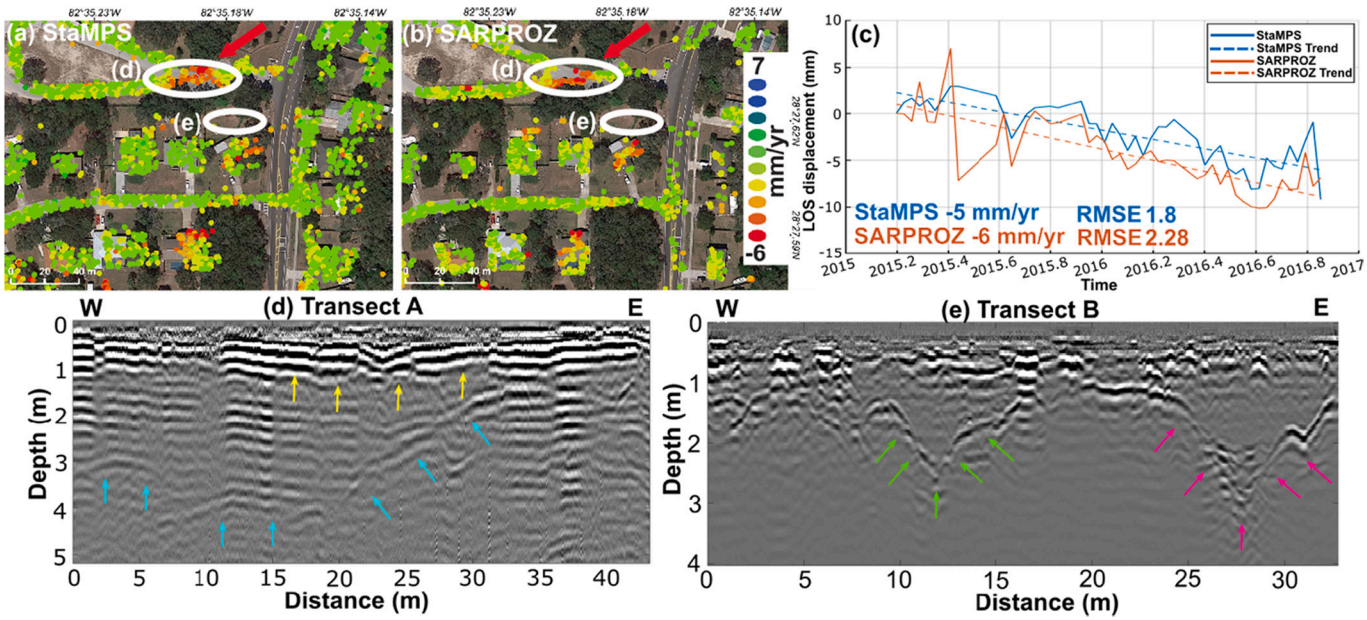

Fig. 9. Velocity maps, InSAR time series, and GPR transects of a section of Site 2. Location shown in Fig. 3. The velocities were determined from TSX ST data covering a time span of 1.7 years and processed by StaMPS (a) and SARPROZ (b) software packages. The red arrow shows the subsiding region from which one scatterer was selected to plot the time series in (c). The white ellipses mark the locations of the two GPR transects shown in (d) and (e). (c) SARPROZ and StaMPS detected movement time series of scatters from the road (marked by red arrows in (a) and (b)) showing deformation velocity of −6 and − 5 mm/yr, respectively. (d) GPR Transect A (within the northernmost ellipse on Fig. 9a and b). The stratigraphy is obscured by antenna ringing effects, but at least 2 distinctive features indicate ongoing depression: a 4-m deep and 35 m wide down-warped layer marked with blue arrows, and a shallower 15-m wide depression marked with yellow arrows. The latter is coincident with the zone of fastest InSAR subsidence (red arrow in (a) and (b)). (e) GPR Transect B (southernmost ellipse in (a) and (b)). This *E*-W GPR profile shows strong reflections between 0.5 and 4 m depth displaying a warping of sediments mantling the limestone that is characteristic of sinkhole activity in West-Central Florida. (For interpretation of the references to colour in this figure legend, the reader is referred to the web version of this article.)

Previous studies successfully used space-borne InSAR to detect sinkhole activity over highly coherent scattering environments (Gutiérrez et al., 2008; Nof et al., 2013, 2019; Chang and Hanssen, 2014; Atzori et al., 2015; Theron et al., 2017; Baer et al., 2018; La Rosa et al., 2018; Martel et al., 2018). In contrast to these studies, this work faced challenges related to the subsidence and scattering characteristics intrinsic to West-Central Florida. First, deformation is limited to very small areas, meters to tens of meters in scale, making the use of high-resolution data highly desirable. Second, ground cover of suburban central Florida is highly vegetated, limiting the observations solely to small patches of built areas. Third, the location of sinkholes is mostly unknown, demanding an extra set of criteria to separate the sinkhole-related signal from other sources of deformation. Finally, ground truthing is difficult, because many of the detected deforming locations lie on private land, requiring the authorization of the owner for ground surveys. As the presence of sinkhole activity may cause devaluation of properties, many homeowners prefer to ignore sinkhole warnings and refuse to conduct ground surveys.

It has been shown that CRs can be used as reference control points as well as to monitor areas with low coherence (Marinkovic et al., 2008; Sousa and Hooper, 2009; Wegmüller et al., 2010; Crosetto et al., 2013). Our results also indicate that CRs successfully improve the phase observations (Fig. 9). The observed improvement of the phase signal suggests that small-size CRs (as the ones used in this work) can be a valuable addition for sinkhole or other hazard monitoring in vegetated areas such as West-Central Florida. However, the use of CRs requires a prior inference of sinkhole activity, which is not always available.

Image resolution plays an important role in detection capability, particularly in Florida where the sinkholes are commonly rather small. Differences in persistent scatterer density are apparent when comparing the high spatial resolution results in Sites 1–3 (Figs. 5–9) and also noticeable in the cluster analysis (Fig. 4). The PS density is strongly related to the sensor's pixel size, but also to the land cover type found in each particular acquisition. To exemplify the impact of resolution in PS detection we performed an analysis of PS candidate density. The SAR backscatter information is used to estimate amplitude stability using a threshold of 0.7 as selection criteria. Different resolutions and sensors were tested to observe the impact that each has on PS selection, and thus the detection of sinkhole movements (Table 3). Amplitude stability provides a good assessment of reliable persistent scatterers, because it is not strongly affected by changes in the atmosphere, topography and acquisition geometry. Amplitude dispersion is measured by the ratio between the standard deviation and the mean of the measured amplitude (Eq. (S3) supplemental material) (Ferretti et al., 2001). Results of the analysis show that Staring Spotlight (ST) acquisition provides considerably more persistent scatterers per unit land area than the other acquisitions. On the other hand, the area covered by a single Staring Spotlight image is smaller, 17.5 km^2, in which each pixel covers an area of 0.15m^2. In order to understand the importance of PS density from data acquired with other spatial resolutions, we also processed COSMO-SkyMed and Sentinel-1 datasets acquired over the study area of western Central Florida. Information about these two datasets and their processing is provided in the Supplementary Materials (S6). The results of

Table 3
Spatial resolution and PS candidate density of SAR data.

Sensor	Mode	Spatial Resolution	Urban coverage %	PS density	
				PS/ km^2	PS/ 100m^2
TSX	ST	0.25 × 0.6 m	60%	69,733	6.973
	HS	1.1 × 0.6 m	52%	6397	0.640
	SL	1.7 × 1.2 m	55%	3836	0.384
CSK	SM	3 × 3 m	52%	961	0.096
Sentinel-1	IW	3.5 × 22 m	26%	152	0.015

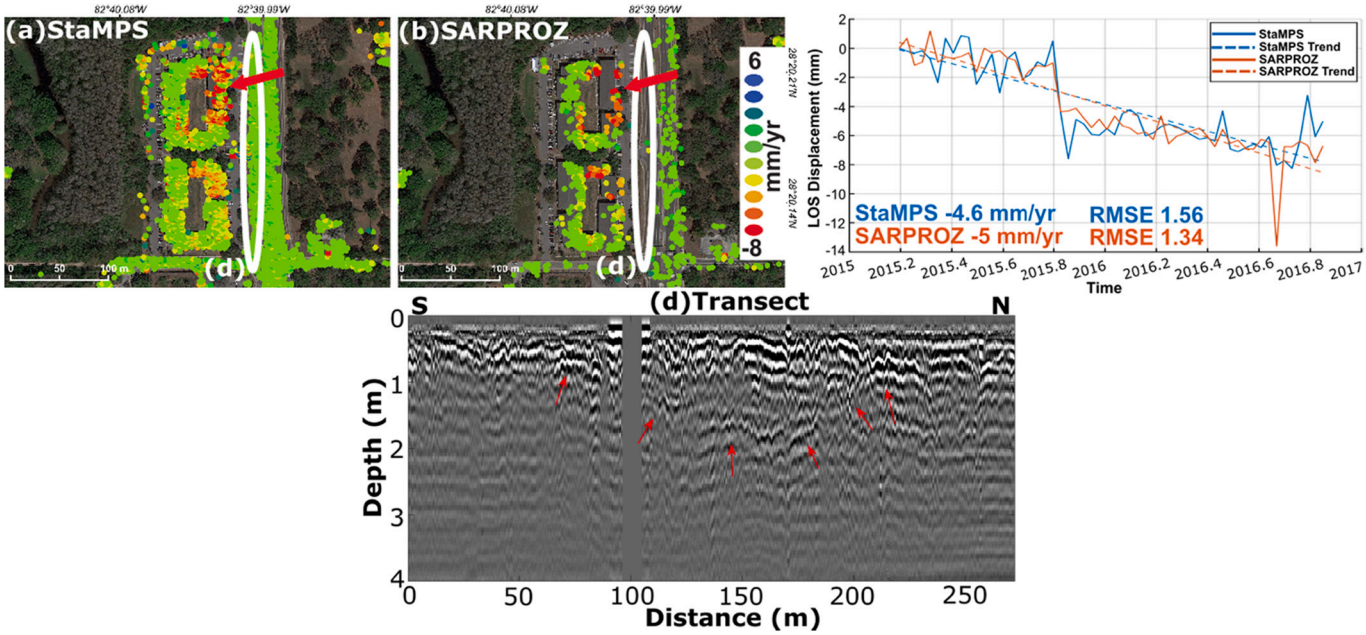

Fig. 10. Velocity map and GPR transect of Ridgestone apartments building on Site 3 determined from TSX ST data covering a time span of 1.7 years, processed using StaMPS and SARPROZ software packages. a) StaMPS velocity field zoom-in to the building showing subsidence in the east zone, covering an area of roughly 1700 m^2. This building has a drainage system to help avoid flooding located in the center. b) SARPROZ velocity field of the same building. c) SARPROZ and StaMPS detected pixel movement time series showing deformation velocity of −5 and − 4.6 mm/yr respectively. The red arrow shows the scatterers plotted in c). d) GPR transect. Red arrows on the GPR profile mark a 150 m-wide 1.8 m deep infilled depression with maximum depth southeast of the zone of concentrated subsiding scatterers on the northern segment of the building. (For interpretation of the references to colour in this figure legend, the reader is referred to the web version of this article.)

the PS density analysis are presented in Table 3 and show a systematic decrease of PS density with reduced spatial resolution. The lowest PS density was found using the Sentinel-1 dataset with pixel size of approximately 55m^2. This dataset was cropped to remove water pixels and keep mostly land cover, leaving an area of 5625 km^2 of coverage over West-Central Florida. An estimation of urban coverage percentage was calculated for all sites using the Florida Land Cover Classification layer (Kawula and Redner, 2018).

Overall, InSAR implementation for detecting sinkhole activity in West-Central Florida has shown to be a promising tool, but still with limitations. Sinkhole collapse can happen in matter of seconds. Thus, the technique detection capability is limited to sinkholes that present subsidence for at least more time than the repeat pass interval of the satellite. It will also be constrained by the relationship between spatial resolution and observed feature size. In West Central Florida for example, given the small sinkhole size (average radius of 3.7 m and a depth of 2 m (Florida Geological Survey, 2015)) and the presence of dense vegetation, the use of high-spatial resolution datasets is desirable (Table 3). The implementation of denser acquisition plans (e.g. shorter satellite repeat pass interval), as well as higher resolution digital elevation models (e.g. LIDAR) will improve detection results, reducing noise in the velocity field and time series (Nof et al., 2013). Ground truthing in west central Florida is a challenging task, as the vast majority of buildings are located in private property, and owners may deny access due to risk of property value loss. Nevertheless, utilizing radar interferometry allows observation of sinkhole-related deformation over large areas, easing the task of locating regions where detailed ground truthing may be desirable.

6. Conclusions

Time series analysis of three TSX frames over 1.75 to 2.5 years in West-Central Florida reveal that small localized deformation was effectively detected using high-resolution InSAR, at sites where buildings or roads presented effective persistent scatterers. The most-rapidly subsiding clusters of PS points in each site moved at average rates of −3 to −6 mm/yr. At each site the most rapidly subsiding cluster was associated with sinkhole deformation. At sites 2 and 3, no prior sinkhole location was known, and GPR surveys confirmed the presence of sinkhole activity. These sites thus demonstrate that PS distribution and clustering analysis could be used to pinpoint deformation signals that proved to be sinkhole-related. Corner Reflectors used on study site 1 effectively enhanced backscattering, allowing subtle (1 mm/yr) sinkhole-related displacements to be measured in a low-coherence region.

A resolution assessment of five different SAR acquisition modes reveals that a medium to high resolution is desired in order to detect possible sinkhole movements. For areas such as suburban Florida, the implementation of high-resolution InSAR analysis may provide crucial and relevant information on sinkhole activity, complementing ground-based methods and helping to better assess sinkhole hazards.

Credit author statement

First author was involved with writing, data processing and interpretation for the paper, Dr. Shimon Wdowinski collaborated with the manuscript writing, structure and science. Dr. Sarah Kruse provided manuscript feedback and collaborated with in-situ interpretations as well as with in-situ measurements. Tonian Robinson provided in-situ interpretations and measurements as well as manuscript feedback.

Declaration of Competing Interest

None.

Acknowledgements

This research was supported by NSF grants EAR-1620617 and EAR-1713420. The authors would like to thank the German Aerospace Center (DLR) for the access to TerraSAR-X imagery through the GEO3330

project, the Italian Space Agency (ASI) for accessing COSMO-SkyMed data, and the European Space Agency (ESA) for accessing Sentinel-1 data. We also thank Daniele Perissin and the SARPROZ team for allowing us to use the software package and UNAVCO for the support for the CR installation and data order. We are grateful to Bruce Rodgers, P. G., for his support in facilitating access for studies and CRs on the Sandhill Scout Reservation. The first author would like to acknowledge Conacyt and Fulbright fellowships for supporting this research. This work is contribution number 1366 from the Institute of Environment at Florida International University.

Appendix A. Supplementary data

Supplementary data to this article can be found online at https://doi.org/10.1016/j.rse.2021.112793.

References

Atzori, S., et al., 2015. InSAR-based modeling and analysis of sinkholes along the Dead Sea coastline. Geophys. Res. Lett. 42 (20), 8383–8390. https://doi.org/10.1002/2015GL066053.

Baer, G., et al., 2018. InSAR measurements and viscoelastic modeling of sinkhole precursory subsidence: implications for sinkhole formation, early warning, and sediment properties. J. Geophys. Res. Earth Surf. 123 (4), 678–693. https://doi.org/10.1002/2017JF004594.

Bürgmann, R., Rosen, P.A., Fielding, E.J., 2000. Synthetic aperture radar interferometry to measure Earth's surface topography and its deformation. Annu. Rev. Earth Planet. Sci. 28 (1), 169–209. https://doi.org/10.1146/annurev.earth.28.1.169.

Chang, L., Hanssen, R.F., 2014. Detection of cavity migration and sinkhole risk using radar interferometric time series. Remote Sensing of Environment. 147, 56–64. https://doi.org/10.1016/j.rse.2014.03.002. Elsevier Inc.

Crosetto, M., et al., 2013. Interferometric SAR monitoring of the Vallcebre landslide (Spain) using corner reflectors. Nat. Hazards Earth Syst. Sci. 13 (4), 923–933. https://doi.org/10.5194/nhess-13-923-2013.

Dobecki, T.L., Upchurch, S.B., 2006. Geophysical applications to detect sinkholes and ground subsidence. Lead. Edge 25 (3), 336. https://doi.org/10.1190/1.2184102.

Downs, C.M., 2017. Imaging Wetland Hydrogeophysics : Applications of Critical Zone Hydrogeophysics to Better Understand Hydrogeologic Conditions in Coastal and Inland Wetlands and Waters by. University of South Florida. Available at: https://scholarcommons.usf.edu/etd/7397.

Ester, M., et al., 1996. A density-based algorithm for discovering clusters in large spatial databases with noise, 96 (34), 226–231. https://doi.org/10.1016/B978-044452701-1.00067-3.

Ferretti, A., Prati, C., Rocca, F., 2001. Permanent Scatterers in SAR interferometry. IEEE Trans. Geosci. Remote Sens. 39 (1), 8–20. https://doi.org/10.1109/36.898661.

Florida Geological Survey, 2015. Florida Subsidence Incidents Reports. Available at: https://floridadep.gov/fgs/sinkholes/content/subsidence-incident-reports.

Florida Office of Insurance Regulation, 2010. Report on Review of the 2010 Sinkhole Data Call. Tallahassee, FL. Available at: https://www.floir.com/siteDocuments/Sinkholes/2010_Sinkhole_Data_Call_Report.pdf.

Ford, D., Williams, P., 2007. Karst hydrogeology and geomorphology. In: Karst Hydrogeology and Geomorphology. John Wiley & Sons, Chichester. https://doi.org/10.1002/9781118684986.

Forth, R.A., Butcher, D., Senior, R., 1999. Hazard mapping of karst along the coast of the Algarve, Portugal. Eng. Geol. 52 (1–2), 67–74. https://doi.org/10.1016/S0013-7952(98)00056-8.

Freeman, A., 1992. Sar calibration: an overview. IEEE Trans. Geosci. Remote Sens. 30 (6), 1107–1121. https://doi.org/10.1109/36.193786.

Frumkin, A., et al., 2011. The Dead Sea sinkhole hazard: Geophysical assessment of salt dissolution and collapse. Geomorphology 134 (1–2), 102–117. https://doi.org/10.1016/j.geomorph.2011.04.023. Elsevier B.V.

Galve, J.P., et al., 2008. Probabilistic sinkhole modelling for hazard assessment. Earth Surf. Process. Landf. 34 (December 2008), 437–452. https://doi.org/10.1002/esp.

Galve, J.P., Remondo, J., Gutiérrez, F., 2011. Improving sinkhole hazard models incorporating magnitude-frequency relationships and nearest neighbor analysis. Geomorphology 134 (1–2), 157–170. https://doi.org/10.1016/j.geomorph.2011.05.020. Elsevier B.V.

Garthwaite, M.C., et al., 2015. The Design of Radar Corner Reflectors for the Australian Geophysical Observing System: a single design suitable for InSAR deformation monitoring and SAR calibration at multiple microwave frequency bands. Geosci. Aust. https://doi.org/10.11636/Record.2015.003. Canberra, (April).

Gutiérrez, F., Cooper, A.H., Johnson, K.S., 2008. Identification, prediction, and mitigation of sinkhole hazards in evaporite karst areas. Environ. Geol. 53 (5), 1007–1022. https://doi.org/10.1007/s00254-007-0728-4.

Gutiérrez, F., et al., 2011. Integrating geomorphological mapping, trenching, InSAR and GPR for the identification and characterization of sinkholes: a review and application in the mantled evaporite Karst of the Ebro Valley (NE Spain). Geomorphology 134 (1–2), 144–156. https://doi.org/10.1016/j.geomorph.2011.01.018. Elsevier B.V.

Herring, T.A., et al., 2016. Reviews of geophysics data analysis methods and geodetic products. Rev. Geophys. 759–808. https://doi.org/10.1002/2016RG000529.

Hooper, A., et al., 2004. A new method for measuring deformation on volcanoes and other natural terrains using InSAR persistent Scatterers. Geophys. Res. Lett. 31 (23), 1–5. https://doi.org/10.1029/2004GL021737.

Jones, C.E., Blom, R.G., 2013. Bayou corne, louisiana, sinkhole: precursory deformation measured by radar interferometry. Geology 42, 111–114. https://doi.org/10.1130/G34972.1.

Kampes, B.M., Hanssen, R.F., Perski, Z., 2003. Radar interferometry with public domain tools. In: Proceedings of FRINGE, pp. 59–68.

Kawula, R., Redner, J., 2018. Florida Cooperative Land Cover [Raster]. Florida Fish and Wildlife Conservation Commission. https://gis.myfwc.com/data/zips/custom/clc/CLC_Raster.zip.

Kim, J.-W., Lu, Z., 2018. Association between localized geohazards in West Texas and human activities, recognized by Sentinel-1A/B satellite radar imagery. Sci. Rep. 8 (1), 4727. https://doi.org/10.1038/s41598-018-23143-6. Springer US.

Kim, Y., Nam, B.H., 2014. A Comparative Study of Karst Sinkhole Hazard Mapping Using Frequency Ratio and Artificial Neural Network for East Central Florida, pp. 105–114.

La Rosa, A., et al., 2018. Growth of a sinkhole in a seismic zone of the northern Apennines (Italy). Nat. Hazards Earth Syst. Sci. 18 (9), 2355–2366. https://doi.org/10.5194/nhess-18-2355-2018.

Marinkovic, P., et al., 2008. InSAR quality control: analysis of five years of corner reflector time series. In: European Space Agency. ESA SP (Special Publication). (649 SP).

Martel, R., et al., 2018. ERT, GPR, InSAR, and tracer tests to characterize karst aquifer systems under urban areas: the case of Quebec City. Geomorphology 310, 45–56. https://doi.org/10.1016/j.geomorph.2018.03.003.

Massonnet, D., Feigl, K.L., 1998. Radar interferometry and its application to changes in the Earth's surface. Rev. Geophys. 4 (36), 441–500.

Nof, R.N., et al., 2013. Sinkhole precursors along the Dead Sea, Israel, revealed by SAR interferometry. Geology 41 (9), 1019–1022. https://doi.org/10.1130/G34505.1.

Nof, R., et al., 2019. SAR interferometry for sinkhole early warning and susceptibility assessment along the Dead Sea, Israel. Remote Sens. 11 (1), 89. https://doi.org/10.3390/rs11010089.

Perissin, D., Wang, Z., Wang, T., 2011. The SARPROZ InSAR tool for urban subsidence/manmade structure stability monitoring in China. In: Proceedings of the ISRSE. Sidney, Australia. Available at: http://www.isprs.org/proceedings/2011/isrse-34/211104015Final00632.pdf.

Robinson, T., Rodgers, B., Oliver-Cabrera, T., Downs, C., Kruse, S., Wdowinski, S., Jazayeri, S., Esmaeili, S., Kiflu, H., 2021. Complex relationships between surface topography, ground motion, and cover sediments in covered karst, West-Central Florida, USA. Geomorphology 392, 107927. https://doi.org/10.1016/j.geomorph.2021.107927. In press.

Rosen, P.A., et al., 2000. Synthetic aperture radar interferometry. Proc. IEEE 88 (3), 333–382.

Sinkhole Type, 1985. Development and Distribution in Florida (1985). U.S. Geological Survey. Available at: http://publicfiles.dep.state.fl.us/OTIS/GIS/data/SINKHOLE_TYPES.zip.

Sousa, J.J., Hooper, A.J., 2009. Comparative study of two different PS-InSAR approaches: DePSI vs. StaMPS. In: Proceedings of the FRINGE 2009 Workshop, 2009 (March).

Theron, A., Engelbrecht, J., 2018. The role of earth observation, with a focus on SAR interferometry, for sinkhole hazard assessment. Remote Sens. 10 (10), 1506. https://doi.org/10.3390/rs10101506.

Theron, A., et al., 2017. Detection of sinkhole precursors through SAR interferometry: radar and geological considerations. IEEE Geosci. Remote Sens. Lett. 14 (6), 871–875. https://doi.org/10.1109/LGRS.2017.2684905.

Tihansky, A.B., 1999. Sinkholes, West-Central Florida. In: Land Subsidence in the United States: US Geological Survey Circular, 1182, pp. 121–140.

Veni, G., Brashear, C.C., Glasbrenner, D., 2014. Building Codes to Minimize Cover Collapses in Sinkhole-Prone Areas (February), pp. 471–476.

Waltham, T., Bell, F.G., Culshaw, M., 2005. Sinkholes and Subsidence: Karst and Cavernous Rocks in Engineering and Construction. Springer Science & Business Media, Berlin/Heidelberg, Germany.

Weary, D.J., 2015. The cost of karst subsidence and sinkhole collapse in the United States compared with other natural hazards. Sinkhole Conference 2015, 433–446. Available at: http://scholarcommons.usf.edu/sinkhole_2015/ProceedingswithProgram/Mgmt_Regs_Education/1.

Weary, D.J., Doctor, D.H., 2014. Karst in the United States: a digital map compilation and database: U.S. In: United States Geological Survey Open-File Report, 1156, p. 23. https://doi.org/10.3133/ofr20141156.

Wegmüller, U., et al., 2010. Nonuniform ground motion monitoring with TerraSAR-X persistent scatterer interferometry. IEEE Trans. Geosci. Remote Sens. 48 (2), 895–904. https://doi.org/10.1109/TGRS.2009.2030792.

Witze, A., 2013. Florida forecasts sinkhole burden. Nature 504 (7479), 196–197. https://doi.org/10.1038/504196a.

Youssef, A.M., El-Kaliouby, H., Zabramawi, Y.A., 2012. Sinkhole detection using electrical resistivity tomography in Saudi Arabia. J. Geophys. Eng. 9 (6), 655–663. https://doi.org/10.1088/1742-2132/9/6/655.

Zebker, H.A., Villasenor, J., 1992. Decorrelation in interferometric radar echoes. IEEE Trans. Geosci. Remote Sens. 30 (5), 950–959. https://doi.org/10.1109/36.175330.